

GrASPE: Graph based Multimodal Fusion for Robot Navigation in Unstructured Outdoor Environments

Kasun Weerakoon, Adarsh Jagan Sathyamoorthy, Jing Liang, Tianrui Guan, Utsav Patel, and Dinesh Manocha
Supplemental version including Tech Report, and Video at <http://gamma.umd.edu/graspe/>

Abstract—We present a novel trajectory traversability estimation and planning algorithm for robot navigation in complex outdoor environments. We incorporate multimodal sensory inputs from an RGB camera, 3D LiDAR, and robot’s odometry sensor to train a prediction model to estimate candidate trajectories’ success probabilities based on partially reliable multi-modal sensor observations. We encode high-dimensional multi-modal sensory inputs to low-dimensional feature vectors using encoder networks and represent them as a connected graph to train an attention-based Graph Neural Network (GNN) model to predict trajectory success probabilities. We further analyze the image and point cloud data separately to quantify sensor reliability to augment the weights of the feature graph representation used in our GNN. During runtime, our model utilizes multi-sensor inputs to predict the success probabilities of the trajectories generated by a local planner to avoid potential collisions and failures. Our algorithm demonstrates robust predictions when one or more sensor modalities are unreliable or unavailable in complex outdoor environments. We evaluate our algorithm’s navigation performance using a Spot robot in real-world outdoor environments. We observe an increase of $x\%$ in terms of success rate and a $y\%$ decrease in false positive estimations compared to the state-of-the-art navigation methods.

I. INTRODUCTION

Mobile robots have increasingly been utilized in numerous outdoor applications such as delivery[1], agriculture[2], surveillance[3], exploration[4], rescue missions[5], etc. These applications need the ability for the robots to navigate challenging outdoor environmental conditions such as inclement weather, low lighting, cluttered vegetation, etc. In this work, we consider such environments as *unstructured outdoor environments*.

The robots’ perception could encounter noise, occlusions, or other mode of error or failures when navigating in such unstructured outdoor environments. Especially, cameras undergo motion blur, low lighting and occlusions [6], [7] while LiDAR point cloud experience heavy distortions in cluttered vegetation. A key issue is to develop methods that can perform reliable perception and planning computations by taking into account such sensor uncertainties.

In terms of robot perception, deep learning (DL) techniques have been proposed for multi-modal sensor fusion. These methods combine distinct feature representations from different sensor modalities such as camera, IMU, and lidar [8], [9], [10], [11] or perform only camera-lidar fusion [12], [13]. Some of these methods use Graph Neural Networks (GNN) [14], which have been used for multi-modal sensor fusion in indoor scenes [15], [16]. A key challenge is to develop reliable methods for outdoor scenes.



Fig. 1: Spot robot navigation in unstructured outdoor terrains using GrASPE.

Moreover, the existing DL and GNN methods do not consider the variable reliability of the cameras and lidars in highly unstructured environments.

In terms of planning in unstructured outdoor environments, the robot must compute trajectories that avoid collisions and prevent the robot from getting stuck (e.g., in vegetation such as bushes, vines, etc). To this end, several recent works have incorporated anomaly detection algorithms to identify collisions or failures during navigation as anomalies based on multi-sensory observations [17], [18], [19]. Such algorithms can be trained using simple positively and negatively labeled samples which can be created trivially as opposed to the extensive labeling required for training supervised learning methods [20], [21], [22]. These positive and negative samples are typically corresponding to traversable and non-traversable observations (e.g. due to possible collisions or other mode of failures). However, since these observations do not account for potential future navigation failures and collisions, such methods could lead to catastrophic accidents during navigation.

To deal with possible future navigation failures due to sensor uncertainties, *proactive anomaly detection* methods have been utilized to estimate the probability of future navigation failure using predicted trajectories, and multi-sensor observations [7], [23]. However, robots navigating in *unstructured outdoor environments* frequently experience

varying lighting conditions, and partial or complete sensor occlusions that lead to distorted sensory observations.

Main Contributions: We present GrASPE (Graph Attention based Sensor fusion for Path Evaluation), a novel trajectory traversability estimation and planning algorithm for legged robot navigation in unstructured outdoor environments. We incorporate multi-modal observations from an RGB camera, 3D LiDAR, and robot odometry to train a prediction model to estimate candidate trajectories’ success probability for navigation. Our model learns the correlation between multi-sensor data under unstructured outdoor conditions where the camera undergoes occlusions, motion-blur, and low-lights while the LiDAR experience heavy point cloud distortions. We further evaluate the reliability of camera and LiDAR inputs to achieve *reliability-aware* multi-modal fusion in our prediction model via a graph attention formulation. The key contributions of our approach include:

- A novel graph-based prediction model that can estimate a given trajectory’s probability of avoiding navigation failures (i.e. success probabilities) such as collisions and getting stuck based on partially reliable multi-modal sensor observations in unstructured outdoor environments. The prediction model is capable of estimating the success probabilities of a trajectory even when the sensory observations are distorted due to varying environmental conditions.
- Novel reliability estimation methods to quantify the usefulness of image and 3D point cloud data for sensor fusion. Our model incorporates feature encoding networks to project high-dimensional sensor inputs into feature vectors. The encoded feature vectors are represented as a connected undirected graph to train an attention-based GNN for sensor fusion. The proposed reliability estimations are employed to augment the weights of this graph representation. In other words, the graph representation is modified with improved *reliability-awareness*.
- A Dynamic Window Approach (DWA) based planner to perform navigation on unstructured outdoor terrains while avoiding potential failures and collisions using our prediction model. The overall pipeline generates dynamically feasible, collision free and traversable actions to navigate a legged robot. We implement our algorithm on a Boston Dynamics *Spot* robot to evaluate its performance in real-world unstructured outdoor scenarios. Our method results in an $x\%$ improvement in terms of success rate compared to state-of-the-art methods.

II. RELATED WORK

In this section, we discuss the existing work on multi-modal sensor fusion and anomaly detection in the context of robot navigation

A. Multi-modal Sensor Fusion for Navigation

Robot perception in real world environments can be challenging due to varying conditions such as lighting, noise,

occlusions, motion blur etc. To this end, prior algorithms incorporate uncertainty modeling and adaptation techniques for robot navigation using a single sensor modality [24], [25]. However, such methods perform well only under controlled outdoor settings, where the given sensor inputs experience limited perturbation in terms of noise from the environment. Therefore, multi-sensor fusion methods are used to deal with real environmental conditions and to mitigate unreliable perception from individual sensors [26], [27], [28]. For instance, different variants of the Kalman Filter [29] are widely used to fuse Odometry (from wheels or visual/LiDAR estimations), IMU, and GPS sensor data to compute improved localization for navigation on slippery and complex terrains [30]. However, these techniques require the different sensors to provide the same type of feature observations (e.g., odometry) which limits their applicability to combine sensors that can provide distinct environmental features (e.g. camera and LiDAR).

Deep learning methods have also been widely used for sensor fusion [26], [28], [31], [32]. Particularly, the camera-lidar fusion is employed in navigation and simultaneous localization and mapping (SLAM)[33] literature to obtain combined perception from visual and geometric features [9], [12]. However, these methods typically assume that both camera and LiDAR perception are reliable in terms of feature availability. In contrast, our proposed algorithm attempts to deal with real unstructured outdoor environments where the above assumption is inapplicable.

B. Anomaly Detection based Prediction Models

Anomaly detection has gained increased attention in recent literature due to the advancements in Deep Learning[34]. Some methods [20] utilize RGB and Depth images as multi-modal observations to train a predictive model that can generate an anomaly mask that reflects ”known” and ”unknown(anomaly)” regions in the scene. However, such methods assume constant illumination and feature-rich image observations for accurate predictions. A supervised variational autoencoder (SVAE) is used [35] for failure identification in unstructured environments using 2D LiDAR data. This SVAE is used [7] as a LiDAR feature encoder to identify navigation anomalies proactively in crop fields using multi-modal fusion. However, the 2D lidar observations are heavily distorted in cluttered outdoor environments such as tall grass and 3D point-cloud can provide richer information, particularly in outdoor scenarios. Other navigation models [36], [21] execute the actions by avoiding undesirable maneuvers in cluttered environments based on the current visual sensory observations. However, such vision-based systems lead to erroneous predictions during camera occlusions and low light conditions. To this end, we propose a camera, 3D LiDAR, and odometry sensor fusion strategy to achieve better perception in unstructured outdoor environments for robot navigation.

III. BACKGROUND AND PROBLEM FORMULATION

In this section, we state the problem formulation and provide background to the Graph Neural Networks (GNNs) used in our approach.

A. Problem Formulation

In this paper, we address the problem of legged robot navigation in *unstructured outdoor environments* using multimodal sensor fusion. We solve the problem in two steps: 1.) Trajectory success probability prediction from multi-modal sensor data 2.) Planning while avoiding unsuccessful trajectories identified using step 1. We incorporate RGB image, 3D Pointcloud, and robot’s velocity history in step 1 to train a prediction model to estimate a given trajectory’s success probability at each time step t as a vector. In this context, we define *success probabilities* as the navigation probability of not encountering collisions, stumbling, or similar modes of failure.

During runtime, a dynamic window approach(DWA) based planner is utilized to generate velocities to reach a goal. However, instead of executing those velocities directly to the robot, we calculate the corresponding future trajectories and feed them to the prediction model along with the multi-sensor data. The prediction model estimates the candidate trajectory’s success probability at each time step t as a vector. Only the velocities corresponding to the trajectories with higher successful probabilities will be executed for planning. Hence, the prediction model trained in step 1 acts as a traversability evaluator for the actions generated by the planner in step 2. The overall system architecture of the prediction model is presented in Fig. 2 and details of our planner are discussed in Section IV-E.

B. Graph Neural Networks (GNNs)

Graph Neural Networks (GNNs) are a class of Neural Networks that can be operated directly on data represented with graphs. In our work, we represent the dimension-reduced multi-sensor features and their reliability measures as a connected graph to learn the correlations between the sensor features. These connections in the graph are mathematically described by a weighted graph $\mathcal{G} := (\mathcal{V}, \mathcal{W})$, where $\mathcal{V} = 1, 2, \dots, N$ is a set of N nodes/vertices associated with elements of the sensors’ feature vectors. \mathcal{W} is a weighted adjacency matrix with entries $\mathcal{W}_{i,j}$ representing the strength of the connection (edge) between feature elements i and j .

We incorporate Graph Convolution Network (GCN) [37] and Graph Attention Network [38] operators in our GNN to encode and pay attention to the local graph structure and node embeddings. GCN is a generalized form of the convolution in CNNs, where the convolution is operated on irregular or non-euclidean data structures (such as graphs) to learn features from a node and its neighbours. We use Graph Attention Network(GAT) [39] to identify the hidden representations of the graph nodes by attending over its neighbors using a self-attention strategy.

IV. PROPOSED METHOD

In this section, we present the details of our proposed navigation algorithm. We first discuss the components of the prediction model trained for trajectory’s success probability estimation: 1. Multi-modal data acquisition and preprocessing, 2. Reduced-dimensional feature representation for multi-modal data, 3. Camera and LiDAR reliability estimation, 4. Graph-based prediction model. Finally, we explain the details of our planning algorithm.

A. Multi-modal Sensors

We design our prediction model (i.e. success probability estimation model) using the following multi-sensor inputs as observations: RGB image $I_t^{rgb} \in \mathbb{R}^{w \times h \times 3}$, 3D pointcloud $P_t^{lidar} \in \mathbb{R}^{3 \times N_p}$, robot’s velocity history $V_t = \{(v, \omega)_{t-T+1}, \dots, (v, \omega)_t\}$ and predicted trajectory from the robot’s current velocity as an image $I_t^{traj} \in \mathbb{R}^{w \times h \times 1}$. To obtain the predicted trajectory image I_t^{traj} , we first extrapolate the robot’s trajectory for the next T times steps based on the current velocity $(v, \omega)_t$. Then, the resulting trajectory is projected to a blank image using the homography projection to generate I_t^{traj} . The RGB image and 3D point cloud captures visual and geometric features of the environment respectively. The robot’s velocity history is used to account for the capture the robot’s recent behavior. Finally, the prediction model incorporates these observations $O_t = [I_t^{rgb}, P_t^{lidar}, V_t, I_t^{traj}]$ and estimates the navigability of the predicted trajectory $\hat{E}_t = [p_t, p_{t+1}, \dots, p_{t+T-1}]$ (i.e. success probability vector). Details of the observation data collection and labeling are described in Section V-B.

B. Multimodal Feature Vector Generation

Different sensor modalities capture different environmental features (images capture visual features, point clouds capture edges and surfaces), and fusing them is not straightforward. Moreover, raw image and point cloud data processing is computationally expensive due to the high dimensionality. Therefore, we process each sensor input using separate feature encoding networks to obtain dimension-reduced feature vector representations.

1) *Visual Feature Extraction*: We utilize a ResNet[42] based pipeline to extract image features f_{img} from the camera RGB image I_t^{rgb} . We incorporate CBAM[43] module between the network layers to perform spatial and channel attention toward the important visual features.

2) *LiDAR Feature Extraction*: Pointnet [44] based network is incorporated to extract pointcloud features f_{point} from the lidar data P_t^{lidar} .

3) *Velocity Feature Extraction*: Velocity vector is fed into a set of linear convolutional layers in VelNet to obtain the velocity features f_{vel} .

4) *Trajectory Feature Extraction*: The predicted trajectory image I_t^{traj} passes through a set of pooling layers and CNN layers to obtain the trajectory feature vector f_{traj} .

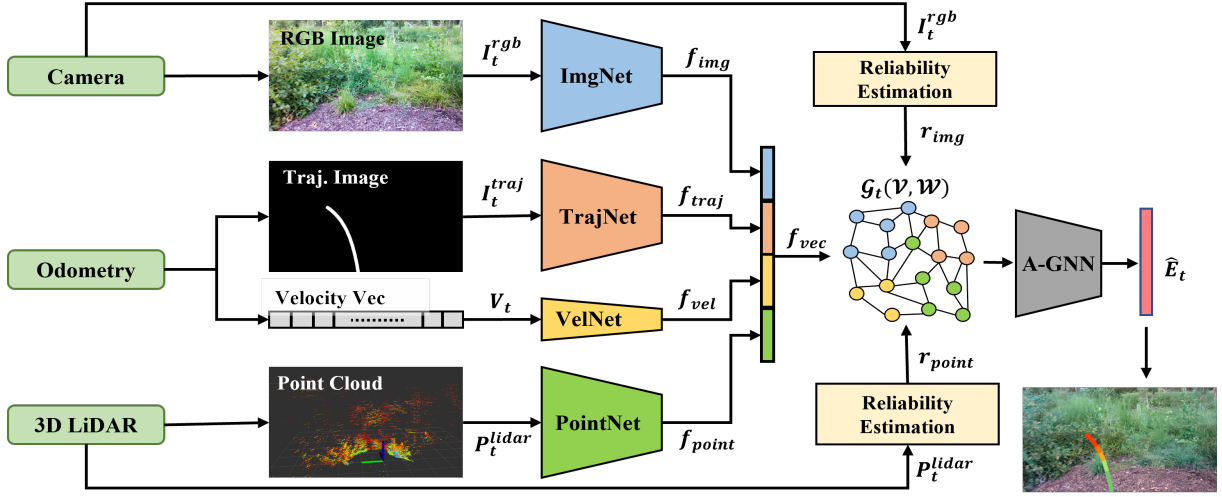


Fig. 2: GrASPE System Architecture for candidate trajectory’s success probability estimation. We utilize RGB image, 3D point cloud, robot’s velocity history, and the predicted trajectory of the robot as an image to train a novel graph based prediction model to estimate the given trajectory’s probably of success in terms of navigation.

C. Sensor Reliability Estimation

We observe that the RGB images and the point cloud data are unreliable in certain unstructured outdoor environments due to the inability of visual and geometric feature detection. Even though the feature encoding networks proposed in the literature and in Section IV-B.1 are capable of feature extraction from images and point clouds, they do not account for the reliability of the input sensory data. To this end, we perform reliability estimation on image and point cloud observations to quantify the reliability as a scalar value.

We estimate the reliability of the image and point cloud inputs at each time step quantitatively using classical image and point processing methods that execute in real-time [45], [46]. We further assume that the instantaneous robot velocities obtained from its odometry are not significantly affected by the environment. Therefore, it is considered as reliable during operation.

1) *Image Reliability Estimation*: We consider that the images captured by the camera have a high reliability if they have: 1. High image brightness, and 2. Availability of visual features such as corners, edges etc [47]. See Fig. 3 for a sample reliability comparison.

To estimate the image brightness, we first convert the input RGB image I_t^{rgb} to a gray-scale image I_t^{gray} . Then we calculate the Root Mean Square(RMS) value of the histogram distribution of I_t^{gray} as follows to obtain brightness estimation,

$$r_{bright} = RMS(hist(I_t^{gray})) \quad (1)$$

Here, $hist$ is the histogram operator and RMS is the root mean square operator where $RMS(x) = \sqrt{\frac{1}{n} \sum_{i=1}^n x_i^2}$.

To estimate the availability of useful features in the image, we calculate the number of corner features n_c in the input image I_t^{rgb} using FAST(Features from Accelerated Segment Test) algorithm proposed in [48], [45]. We consider the image is feature rich if the n_c is higher than a threshold. Hence, $r_{corners} = \frac{n_c}{(w \times h)}$. Here, w and h are the height and

width of the input RGB image. The final image reliability measure is obtained as a normalized scalar value $r_{img} \in [0, 1]$ using the weighted sum of r_{bright} and $r_{corners}$:

$$r_{img} = \alpha_b r_{bright} + \alpha_c r_{corners} \quad (2)$$

2) *Pointcloud Reliability*: We observe that the lidar point cloud is heavily distorted in the presence of unstructured vegetation leading to poor estimation of the surrounding objects’ geometry. Therefore, to evaluate the point cloud reliability, we perform edge and planar feature extraction to calculate the number of 3D features available in the point cloud P_t^{lidar} at a given time t .

Let l be a 3D point in the input point cloud P_t^{lidar} and \mathcal{M} be the set of coordinates of point l acquired from a single LiDAR scan. Then, we can obtain the point feature evaluation factor c_l of the point l as,

$$c_l = \frac{1}{\|X_l\| \cdot |\mathcal{M}|} \left\| \sum_{k \in \mathcal{M}, k \neq l} (X_l - X_k) \right\|, \quad (3)$$

where, X_k with $k = 1, 2, \dots, |\mathcal{M}|$ are the coordinates of the 3D points in the set \mathcal{M} . Zhang et al. [46] demonstrate that the points with higher and lower c_l values obtained from the equation 3 belong to edge and planar features respectively. Hence, we define two threshold values c_{max} and c_{min} to extract the edge and planar points using c_l . The resulting edge and planar feature point sets can be denoted as: $\mathcal{S}_{edge} = \{l | c_l \geq c_{max}, l \in P_t^{lidar}\}$ and $\mathcal{S}_{planar} = \{l | c_l \leq c_{min}, l \in P_t^{lidar}\}$ respectively.

Then, the point cloud reliability measures, r_{edge} and r_{planar} , are calculated using the ratio between the cardinality of each feature point set and the input point cloud.

$$r_{edge} = \frac{|\mathcal{S}_{edge}|}{|P_t^{lidar}|}, \quad r_{planar} = \frac{|\mathcal{S}_{planar}|}{|P_t^{lidar}|}. \quad (4)$$

Finally, the point cloud reliability measure r_{point} is derived as a weighted combination of r_{edge} and r_{planar} using two

tunable parameters β_e and β_p .

$$r_{point} = \beta_e r_{edge} + \beta_p r_{planar}. \quad (5)$$

Fig. 4 presents an example comparison of r_{edge} and r_{planar} in real outdoor scenarios.

D. Graph Attention based Prediction Model

Once the sensor inputs are encoded into feature vectors (Section IV-B), we concatenate them to obtain a combined vector $f_{vec} = [f_{img}, f_{point}, f_{traj}, f_{vel}]$. This $f_{vec} \in [0, 1]^N$ is utilized to generate the graph representation for fusion.

Let $\mathcal{G}_t := (\mathcal{V}, \mathcal{W})_t$ be a graph defined in III-B at time t . We consider the graph nodes $\mathcal{V} = 1, 2, \dots, N$ as a set of N nodes/vertices associated with elements of the feature vector f_{vec} . Then, we define the feature vector f_{vec} as the graph signal residing on the graph nodes \mathcal{V} . i.e. the i^{th} component of the vector f_{vec} denotes the value at the i^{th} node in \mathcal{V} .

The weighted adjacency matrix \mathcal{W} should represent the strength between the graph nodes (i.e. edge weights) i.e. the connectivity between the encoded feature elements in f_{vec} . Typically, the edge weights are calculated using a distance measure (absolute difference or L2 norm). However, we modify this edge weights (especially between the nodes corresponding to the image and point cloud features) based on the reliability measures (Section IV-C) as follows.

Let $\mathcal{W}_{i,j}$ be the edge weight between the feature elements i and j in f_{vec} .

$$\mathcal{W}_{i,j} = \begin{cases} \exp\{-\lambda |f_{vec}(i) - f_{vec}(j)| \times r_{i,j}\}, & \text{if } i \neq j \\ 0, & \text{otherwise,} \end{cases} \quad (6)$$

where, λ is a tunable scalar and $r_{i,j} \in [0, 1]$ represents the reliability measure between the node i and j as follow,

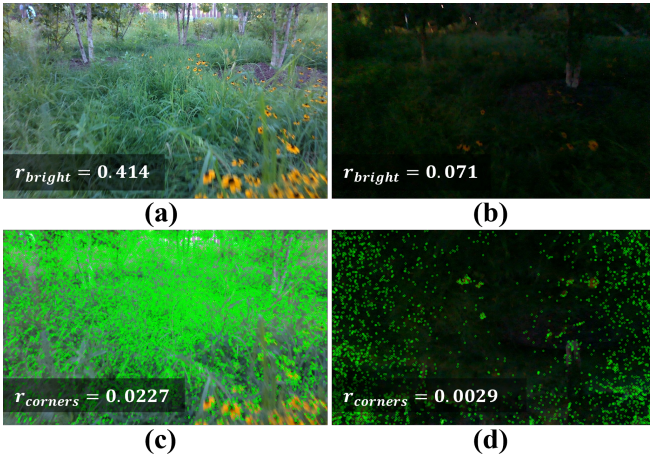


Fig. 3: **Image Reliability Estimation:** We estimate input image reliability based on two factors: 1. Overall lighting condition 2. Feature richness. (a) and (b) demonstrate images of the same scene under two different lighting conditions. (c) and (d) presents the FAST features extracted from the images (a) and (b). We observe that the images obtained under low light conditions have a significantly less number of features. Similarly, the motion blur and camera occlusions result in images with low reliability measures. (see [] cite arxiv version for detailed results).

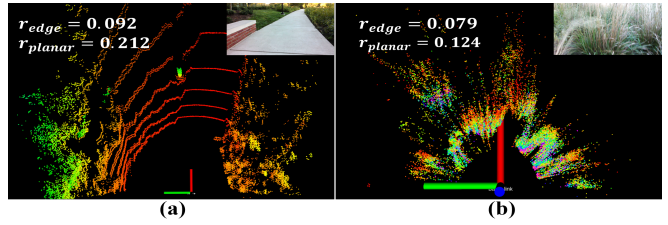


Fig. 4: **Point cloud Reliability Estimation:** We estimate point cloud reliability based on the edge and planar feature availability. (a) Top view of a feature-rich point cloud observation (b) Top view of a distorted point cloud observed in tall grass environments. We observe that the 3D point cloud is feature-rich in open and structured outdoor environments. However, the cluttered vegetation leads to heavy distortions in the point cloud.

$$r_{i,j} = \begin{cases} r_{img}, & \text{if } \{i, j\} \in f_{img}, j \notin f_{point} \\ r_{point}, & \text{if } \{i, j\} \notin f_{img}, j \in f_{point} \\ \frac{1}{2}(r_{point} + r_{img}), & \text{if } \{i, j\} \in f_{img}, j \in f_{point} \\ 1, & \text{otherwise.} \end{cases} \quad (7)$$

Hence, we refer the derived graph representation \mathcal{G}_t of the feature vector f_{vec} as *reliability-aware* feature graph. We design a light-weight Graph Neural Network with a set of Graph Convolution and Graph Attention layers defined in III-B to predict the navigability estimation vector \hat{E}_t for a given trajectory using the *reliability-aware* feature graph \mathcal{G}_t . The overall prediction pipeline can be treated as a mapping function $\psi : \mathcal{O}_t \rightarrow \hat{E}_t$.

E. Outdoor Navigation with DWA

We adapt a modified version of the well-known Dynamic Window Approach (DWA) [49] to perform navigation while evaluating the navigability of the generated trajectories using GrASPE.

We represent the robot's actions as a linear and angular velocity pairs (v, ω) . Let V_s be the space of all the possible robot velocities. The DWA algorithm considers two velocity space constraints to obtain dynamically feasible and collision-free velocities: (1). The dynamic window V_d contains the dynamically feasible velocities during the next Δt time window; (2). The admissible velocity space V_a includes the collision-free velocities. The restricted velocity space $V_r = V_s \cap V_d \cap V_a$.

These collisions for V_a are generally identified by evaluating the potential future trajectory collisions using 2D LiDAR scan data. However, the LiDAR scan is highly distorted and unreliable in cluttered outdoor terrains such as thin grass and vegetation. Hence, the traditional DWA will identify traversable cluttered regions as obstacles. To avoid such misclassifications, we omit the admissible velocity space constraint when the point cloud is highly unreliable.

$$V_r = \begin{cases} V_s \cap V_d, & \text{if } r_{point} \leq r_{th} \\ V_s \cap V_d \cap V_a & \text{otherwise,} \end{cases} \quad (8)$$

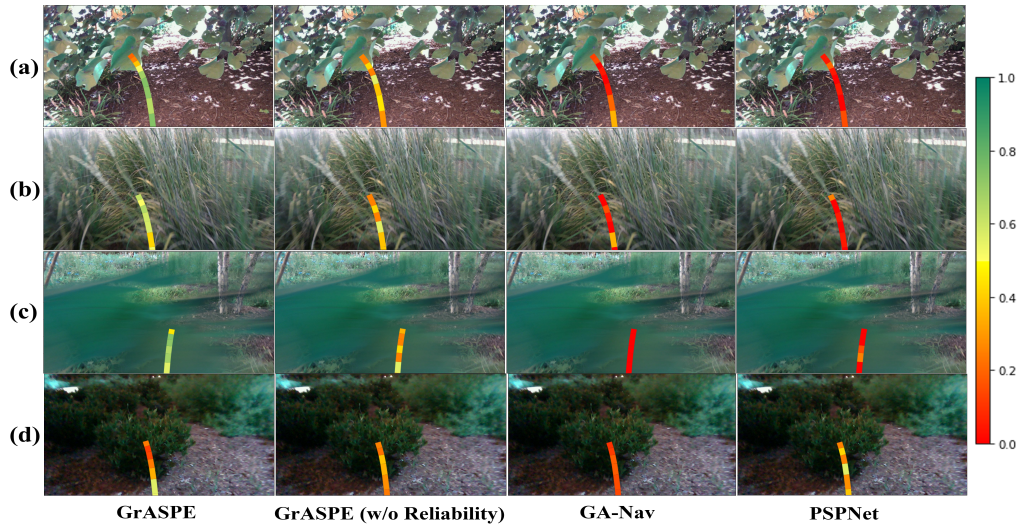


Fig. 5: Navigability predictions from our GrASPE algorithm, GrASPE w/o reliability, GA-Nav[40], and PSPNet[41] under different environmental conditions. (a) Hanging leaves; (b) Pliable tall grass; (c) Camera occlusion; (d) Low-light condition. We observe that the GrASPE algorithm predictions outperform all the other comparison methods under varying environmental conditions that are critical for robot navigation in unstructured outdoor environments.

where r_{th} is a reliability threshold that indicates the point cloud data is highly distorted. The resulting velocity space V_r is utilized to calculate the optimal velocity pair (v^*, ω^*) by maximizing the objective function below,

$$Q(v, \omega) = \sigma(\gamma_1 \cdot \text{heading}(v, \omega) + \gamma_2 \cdot \text{dist}(v, \omega) + \gamma_3 \cdot \text{vel}(v, \omega)), \quad (9)$$

where $\text{heading}(\cdot)$, $\text{dist}(\cdot)$ and $\text{vel}(\cdot)$ are the cost functions [49] to quantify the robot's heading towards the goal, distance to the closest obstacle in the trajectory, and the forward velocity of the robot. σ is a smoothing function and $\gamma_i, i = 1, 2, 3$ are adjustable weights. The resulting optimal velocity pair can be denoted as $(v^*, \omega^*) = \text{argmax}(Q(v, \omega))$.

We calculate the predicted trajectory for the next T time steps considering the optimal (v^*, ω^*) as the robot's immediate next velocity. Then, the obtained trajectory is fed into our GrASPE algorithm to estimate the trajectories' success probabilities \hat{E}_t . If $\min(\hat{E}_t) \geq e_{th}$ and $\text{mean}(\hat{E}_t) \geq e_{th}$, the velocity pair (v^*, ω^*) corresponding to that trajectory is considered as navigable. Otherwise, the (v^*, ω^*) is removed from velocity space V_r and a new optimal velocity pair is calculated using the objective function defined in equation 9. Here, e_{th} is an adjustable threshold.

V. RESULTS AND ANALYSIS

We explain our method's implementation and experimental details on a Spot robot. Then, we conduct ablation studies and comparisons to highlight benefits of our algorithm.

A. Implementation

GrASPE algorithm is implemented using PyTorch and PyTorch Geometric(PyG). The prediction model is trained in a workstation with an Intel Xeon 3.6 GHz processor and

an Nvidia Titan GPU using the data collected from a Spot robot. The robot is equipped with an Intel NUC 11 (a mini PC with Intel i7 CPU and NVIDIA RTX 2060 GPU), a VLP16 Velodyne LiDAR and a L515 Intel RealSense LiDAR Camera.

B. Dataset

RGB image I_t^{rgb} and the point cloud P_t^{lidar} are obtained from the aforementioned camera and the LiDAR respectively. The robot's velocity history V_t is collected from the odometry. The ground truth labels E_t are generated manually using element-wise binary labeling for simplicity. i.e. the traversable portion of the predicted trajectory is labeled as 1's and the non-traversable or possible failure regions are labeled with 0's. We incorporate a randomized planner during the data collection to minimize the human intervention. Hence the observations corresponding to the successful navigation scenarios are automatically labeled using E_t vectors with all 1's. However, the non-traversable or failure cases were manually labeled by evaluating the observations after the data collection. The final dataset includes a set of observation and label pairs (O_t, E_t) for each time step t . The test and training data sets are collected in University of Maryland outdoor fields. The training set includes 28721 positive samples and 8463 negative samples whereas the test set contains 4537 positive samples and 1096 negative samples.

C. Evaluations

We use following evaluation metrics to compare our method's performance against three state of the art navigation methods: GA-Nav[40], PSPNet[41] and DWA[49]. We further compare GrASPE model without reliability estimations for ablation studies. GA-Nav is a multi-modal navigation framework that combines vision-based terrain segmentation with point cloud based elevation estimation for outdoor

navigation. PSPNet is a vision based segmentation algorithm trained for outdoor terrain segmentation. DWA is a local planner that utilizes 2D LiDAR scan for obstacle avoidance. **Success Rate** - The number of successful goal reaching attempts (while avoiding non-pliable regions and collisions) over the total number of trials.

Normalized Trajectory length - The ratio between the robot's trajectory length and the straight-line distance to the goal in both successful and unsuccessful trajectories.

VI. CONCLUSIONS, LIMITATIONS AND FUTURE WORK

REFERENCES

- [1] R. Limosani, R. Esposito, A. Manzi, G. Teti, F. Cavallo, and P. Dario, "Robotic delivery service in combined outdoor-indoor environments: technical analysis and user evaluation," *Robotics and autonomous systems*, vol. 103, pp. 56–67, 2018.
- [2] J. J. Roldán, J. del Cerro, D. Garzón-Ramos, P. Garcia-Aunon, M. Garzón, J. De León, and A. Barrientos, "Robots in agriculture: State of art and practical experiences," *Service robots*, pp. 67–90, 2018.
- [3] M. Z. Zaheer, A. Mahmood, M. H. Khan, M. Astrid, and S.-I. Lee, "An anomaly detection system via moving surveillance robots with human collaboration," in *Proceedings of the IEEE/CVF International Conference on Computer Vision*, 2021, pp. 2595–2601.
- [4] Y. Gu, J. Strader, N. Ohi, S. Harper, K. Lassak, C. Yang, L. Kogan, B. Hu, M. Gramlich, R. Kavi, *et al.*, "Robot foraging: Autonomous sample return in a large outdoor environment," *IEEE Robotics & Automation Magazine*, vol. 25, no. 3, pp. 93–101, 2018.
- [5] B. Choi, W. Lee, G. Park, Y. Lee, J. Min, and S. Hong, "Development and control of a military rescue robot for casualty extraction task," *Journal of Field Robotics*, vol. 36, no. 4, pp. 656–676, 2019.
- [6] M. Aladem, S. Baek, and S. A. Rawashdeh, "Evaluation of image enhancement techniques for vision-based navigation under low illumination," *Journal of Robotics*, vol. 2019, 2019.
- [7] T. Ji, A. N. Sivakumar, G. Chowdhary, and K. Driggs-Campbell, "Proactive anomaly detection for robot navigation with multi-sensor fusion," *IEEE Robotics and Automation Letters*, vol. 7, no. 2, pp. 4975–4982, 2022.
- [8] A. J. Sathyamoorthy, K. Weerakoon, T. Guan, J. Liang, and D. Manocha, "Terrapn: Unstructured terrain navigation through online self-supervised learning," *arXiv preprint arXiv:2202.12873*, 2022.
- [9] S. S. Mansouri, C. Kanellakis, D. Kominiak, and G. Nikolakopoulos, "Deploying mavs for autonomous navigation in dark underground mine environments," *Robotics and Autonomous Systems*, vol. 126, p. 103472, 2020.
- [10] K. Weerakoon, A. J. Sathyamoorthy, U. Patel, and D. Manocha, "Terp: Reliable planning in uneven outdoor environments using deep reinforcement learning," in *2022 International Conference on Robotics and Automation (ICRA)*, 2022, pp. 9447–9453.
- [11] K. Weerakoon, S. Chakraborty, N. Karapetyan, A. J. Sathyamoorthy, A. S. Bedi, and D. Manocha, "Htron: Efficient outdoor navigation with sparse rewards via heavy tailed adaptive reinforce algorithm," *arXiv preprint arXiv:2207.03694*, 2022.
- [12] P. Cai, S. Wang, Y. Sun, and M. Liu, "Probabilistic end-to-end vehicle navigation in complex dynamic environments with multimodal sensor fusion," *IEEE Robotics and Automation Letters*, vol. 5, no. 3, pp. 4218–4224, 2020.
- [13] C. Debeunne and D. Vivet, "A review of visual-lidar fusion based simultaneous localization and mapping," *Sensors*, vol. 20, no. 7, p. 2068, 2020.
- [14] Z. Wu, S. Pan, F. Chen, G. Long, C. Zhang, and S. Y. Philip, "A comprehensive survey on graph neural networks," *IEEE transactions on neural networks and learning systems*, vol. 32, no. 1, pp. 4–24, 2020.
- [15] S. Casas, C. Gulino, R. Liao, and R. Urtasun, "Spagnn: Spatially-aware graph neural networks for relational behavior forecasting from sensor data," in *2020 IEEE International Conference on Robotics and Automation (ICRA)*, 2020, pp. 9491–9497.
- [16] Z. Ravichandran, L. Peng, N. Hughes, J. D. Griffith, and L. Carlone, "Hierarchical representations and explicit memory: Learning effective navigation policies on 3d scene graphs using graph neural networks," in *2022 International Conference on Robotics and Automation (ICRA)*. IEEE, 2022, pp. 9272–9279.
- [17] T. Ji, S. T. Vuppala, G. Chowdhary, and K. Driggs-Campbell, "Multimodal anomaly detection for unstructured and uncertain environments," in *Conference on Robot Learning*. PMLR, 2021, pp. 1443–1455.
- [18] D. Park, H. Kim, and C. C. Kemp, "Multimodal anomaly detection for assistive robots," *Autonomous Robots*, vol. 43, no. 3, pp. 611–629, 2019.
- [19] S. Zhou, J. Xi, M. W. McDaniel, T. Nishihata, P. Salesses, and K. Iagnemma, "Self-supervised learning to visually detect terrain surfaces for autonomous robots operating in forested terrain," *Journal of Field Robotics*, vol. 29, no. 2, pp. 277–297, 2012.
- [20] L. Wellhausen, R. Ranftl, and M. Hutter, "Safe robot navigation via multi-modal anomaly detection," *IEEE Robotics and Automation Letters*, vol. 5, no. 2, pp. 1326–1333, 2020.
- [21] G. Kahn, P. Abbeel, and S. Levine, "Badgr: An autonomous self-supervised learning-based navigation system," *IEEE Robotics and Automation Letters*, vol. 6, no. 2, pp. 1312–1319, 2021.
- [22] K. Jin, H. Wang, C. Liu, Y. Zhai, and L. Tang, "Graph neural network based relation learning for abnormal perception information detection in self-driving scenarios," in *2022 International Conference on Robotics and Automation (ICRA)*. IEEE, 2022, pp. 8943–8949.
- [23] M. Sorokin, J. Tan, C. K. Liu, and S. Ha, "Learning to navigate sidewalks in outdoor environments," *IEEE Robotics and Automation Letters*, vol. 7, no. 2, pp. 3906–3913, 2022.
- [24] K. Katyal, K. Popek, C. Paxton, P. Burlina, and G. D. Hager, "Uncertainty-aware occupancy map prediction using generative networks for robot navigation," in *2019 International Conference on Robotics and Automation (ICRA)*, 2019, pp. 5453–5459.
- [25] L. Rusli, B. Nurhalim, and R. Rusyadi, "Vision-based vanishing point detection of autonomous navigation of mobile robot for outdoor applications," *Journal of Mechatronics, Electrical Power, and Vehicular Technology*, vol. 12, no. 2, pp. 117–125, 2021.
- [26] F. Liu, X. Li, S. Yuan, and W. Lan, "Slip-aware motion estimation for off-road mobile robots via multi-innovation unscented kalman filter," *IEEE Access*, vol. 8, pp. 43 482–43 496, 2020.
- [27] Y. Yan, B. Zhang, J. Zhou, Y. Zhang, X. Liu, *et al.*, "Real-time localization and mapping utilizing multi-sensor fusion and visual-imu-wheel odometry for agricultural robots in unstructured, dynamic and gps-denied greenhouse environments," *Agronomy*, vol. 12, no. 8, p. 1740, 2022.
- [28] Y. Qu, M. Yang, J. Zhang, W. Xie, B. Qiang, and J. Chen, "An outline of multi-sensor fusion methods for mobile agents indoor navigation," *Sensors*, vol. 21, no. 5, p. 1605, 2021.
- [29] G. Welch, G. Bishop, *et al.*, "An introduction to the kalman filter," 1995.
- [30] A. E. B. Velasquez, V. A. H. Higtuti, M. V. Gasparino, A. N. Sivakumar, M. Becker, and G. Chowdhary, "Multi-sensor fusion based robust row following for compact agricultural robots," *arXiv preprint arXiv:2106.15029*, 2021.
- [31] Y. Su, T. Wang, S. Shao, C. Yao, and Z. Wang, "Gr-loam: Lidar-based sensor fusion slam for ground robots on complex terrain," *Robotics and Autonomous Systems*, vol. 140, p. 103759, 2021.
- [32] J. Liang, K. Weerakoon, T. Guan, N. Karapetyan, and D. Manocha, "Adaptiveon: Adaptive outdoor navigation method for stable and reliable motions," *arXiv preprint arXiv:2205.03517*, 2022.
- [33] Y.-S. Shin, Y. S. Park, and A. Kim, "Direct visual slam using sparse depth for camera-lidar system," in *2018 IEEE International Conference on Robotics and Automation (ICRA)*. IEEE, 2018, pp. 5144–5151.
- [34] D. Park, H. Kim, and C. C. Kemp, "Multimodal anomaly detection for assistive robots," *Autonomous Robots*, vol. 43, no. 3, pp. 611–629, 2019.
- [35] T. Ji, S. T. Vuppala, G. Chowdhary, and K. Driggs-Campbell, "Multimodal anomaly detection for unstructured and uncertain environments," in *Conference on Robot Learning*. PMLR, 2021, pp. 1443–1455.
- [36] G. Kahn, P. Abbeel, and S. Levine, "Land: Learning to navigate from disengagements," *IEEE Robotics and Automation Letters*, vol. 6, no. 2, pp. 1872–1879, 2021.
- [37] M. Welling and T. N. Kipf, "Semi-supervised classification with graph convolutional networks," in *J. International Conference on Learning Representations (ICLR 2017)*, 2016.
- [38] K. K. Thekumparampil, C. Wang, S. Oh, and L.-J. Li, "Attention-based graph neural network for semi-supervised learning," *arXiv preprint arXiv:1803.03735*, 2018.

- [39] D. Busbridge, D. Sherburn, P. Cavallo, and N. Y. Hammerla, "Relational graph attention networks," *arXiv preprint arXiv:1904.05811*, 2019.
- [40] T. Guan, D. Kothandaraman, R. Chandra, A. J. Sathyamoorthy, K. Weerakoon, and D. Manocha, "Ga-nav: Efficient terrain segmentation for robot navigation in unstructured outdoor environments," *IEEE Robotics and Automation Letters*, vol. 7, no. 3, pp. 8138–8145, 2022.
- [41] H. Zhao, J. Shi, X. Qi, X. Wang, and J. Jia, "Pyramid scene parsing network," in *2017 IEEE Conference on Computer Vision and Pattern Recognition (CVPR)*, 2017, pp. 6230–6239.
- [42] K. He, X. Zhang, S. Ren, and J. Sun, "Deep residual learning for image recognition," in *Proceedings of the IEEE conference on computer vision and pattern recognition*, 2016, pp. 770–778.
- [43] S. Woo, J. Park, J.-Y. Lee, and I. S. Kweon, "Cbam: Convolutional block attention module," in *Proceedings of the European conference on computer vision (ECCV)*, 2018, pp. 3–19.
- [44] C. R. Qi, H. Su, K. Mo, and L. J. Guibas, "Pointnet: Deep learning on point sets for 3d classification and segmentation," in *Proceedings of the IEEE conference on computer vision and pattern recognition*, 2017, pp. 652–660.
- [45] E. Rosten, R. Porter, and T. Drummond, "Faster and better: A machine learning approach to corner detection," *IEEE transactions on pattern analysis and machine intelligence*, vol. 32, no. 1, pp. 105–119, 2008.
- [46] J. Zhang and S. Singh, "Loam: Lidar odometry and mapping in real-time," in *Robotics: Science and Systems*, vol. 2, no. 9. Berkeley, CA, 2014, pp. 1–9.
- [47] A. Mojsilovic, J. Gomes, and B. E. Rogowitz, "Isee: Perceptual features for image library navigation," in *Human Vision and Electronic Imaging VII*, vol. 4662. SPIE, 2002, pp. 266–277.
- [48] E. Rosten and T. Drummond, "Machine learning for high-speed corner detection," in *European conference on computer vision*. Springer, 2006, pp. 430–443.
- [49] D. Fox, W. Burgard, and S. Thrun, "The dynamic window approach to collision avoidance," *IEEE Robotics & Automation Magazine*, vol. 4, no. 1, pp. 23–33, 1997.